International Journal of Thermofluids 24 (2024) 100852

Contents lists available at ScienceDirect

International Journal of Thermofluids

journal homepage: www.sciencedirect.com/journal/international-journal-of-thermofluids

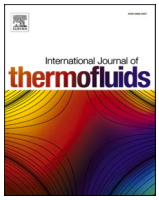

Numerical analysis of magnetohydrodynamic mixed convection and entropy generation in a curvelinear lid-driven cavity with carbon nanotubes and an adiabatic cylinder

Mohammed Azeez Alomari [a,b,*], Qusay H. Al-Salami [c], Farah Q. A. Alyousuf [d], Faris Alqurashi [e], Mujtaba A. Flayyih [f]

[a] Department of Mechanical Engineering, University of Al-Qadisiyah, Ad-Diwaniyah, 58001, Iraq
[b] College of Engineering, University of Warith Al-Anbiyaa, Karbala, Iraq
[c] Department of Business Administration, College of Administrative and Financial Sciences, Cihan University-Erbil, Iraq
[d] Department of Computer Network, College of Engineering and Computer Science, Lebanese French University, Erbil, Kurdistan Region, Iraq
[e] Mechanical Engineering Department, College of Engineering, University of Bisha, Bisha, Saudi Arabia
[f] Biomedical Engineering Department, College of Engineering and Technologies, Al-Mustaqbal University, Hillah, Iraq

ARTICLE INFO

Keywords:
Curvilinear enclosure
Lid-driven
CNT
Inclined MHD
Mixed convection
Entropy generation

ABSTRACT

Mixed convection convection is a vital subject and it is beneficial in many engineering applications. The current paper addresses this subject with a novel geometry and very vital variables including magnetohydrodynamic influences on the forced/free convection as well as the reproduction of irreversibilities in an enclosure filled with water/carbon nanotubes (CNT) and a nonadiabatic cylinder. The top wall is split from the middle and moves in different directions to drive the isotherms which are generated from the bottom wall and cold from the vertical surfaces. The numerical analysis was carried out using finite element method; the variables are Reynolds number (40–200), Richardson number (0.01–10), Hartmann number (0–62), inclined magnetohydrodynamic angle (0–60), volume concentration (0–0.08) while Prandtl number has kept constant at 6.2. The results show that the transformation of heat, as well as the fluid flow, are largely influenced by the change of variables, where increasing Reynolds number, Richardson number enhances heat and increases the flow circulation. Furthermore, heat transfer enhances by 57 % when increasing Ri from 0.1 to 10 at Re=41 and this enhancement increases to 62.5 % at Re = 200. Furthermore, increasing the concentration of the carbon nanotube can cause heat transfer but decrease the circulation of the fluid. In contrast, the transfer of heat as well as the flow streams are remarkably decreased with the increase of the Hartmann at zero inclination angle; however, the value of the Nusselt average increases with the increase of the inclination angle. Moreover, the value of Nusselt average decreses by 34.7 % when increasing Ha from 0 to 62 at Re = 200. Furthermore, the total entropy generation increases as Richardson number, Reynolds number, and volume concentration increase; in contrast, detraction with the rise of the MHD.

1. Introduction

There are lots of papers which have searched to investigate the mixed convection phenomena due to its importance in uncountable engineering applications [1–4], large cooling applications [5,6], small cooling applications [7,8], nuclear power plant [9–12], renewable energy applications [13–17].

Mixed convection in different applications means different geometries to be investigated [18–22]. Combined convection in a trapezoidal enclosure lid drive contains an obstacle was numerically studied by Shah et al. [23]. Richardson number (Ri) and Reynolds number (Re) are some variables which were considered by authors. The enhancement of thermal transformation, according to the authors results, increased as Ri and bouncy ratio increase while declined with the rise of Re. Ruvo et al. [24] studied the combined convection in a T enclosure filled with nonfluid. A range of, Re and Ri were analyzed to understand their effect on the fluid flow and heat transformation. The

* Corresponding author at: Department of Mechanical Engineering, University of Al-Qadisiyah, Ad-Diwaniyah, 58001, Iraq.
E-mail addresses: mohammed.hasan@qu.edu.iq (M.A. Alomari), qusay.hameed@cihanuniversity.edu.iq (Q.H. Al-Salami), frhalyousuf@lfu.edu.krd (F.Q. A. Alyousuf), fars421@hotmail.com (F. Alqurashi), mujtaba_abdulkadhim@uomus.edu.iq (M.A. Flayyih).

https://doi.org/10.1016/j.ijft.2024.100852

Available online 6 September 2024

Nomenclature

B_o	The applied magnetic field (T)
C_p	Specific heat ($Jkg^{-1}C^{o\,-\,1}$)
g	Gravitational acceleration (ms^{-2})
Gr	Grashof number
k	Thermal conductivity (W m^{-1} K^{-1})
ρ	Density (kg/m^3)
Nu	Nusselt number
p	Dimensional pressure
P	Dimensionaless pressure
Pr	Prandtl number
Re	Reynolds number
Ri	Richardson number
∅	Volume concentration
S	Entropy generation
T	Dimensional temperature (C^o)
u	Dimention velocity in x-direction (m.s^{-1})
U	Dimensionless velocity component X-direction
v	Dimention velocity in y-direction (m.s^{-1})
V	Dimensionless velocity component Y-direction
X	Dimensionless X-coordinates
W	Dimensionless enclosure hight
Y	Dimensionaless Y-coordinates
α	thermal diffusivity ($\frac{m^2}{s}$)
σ	electrical conductivity (S m^{-1})
β_o	thermal expansion coefficient (T^{-1})
μ	Dynamic viscosity ($\frac{kg}{m.s}$)
θ	Dimensionless temperature
Ψ	Absolute stream function

Subscripts

l	low
h	high
avg	average
loc	local

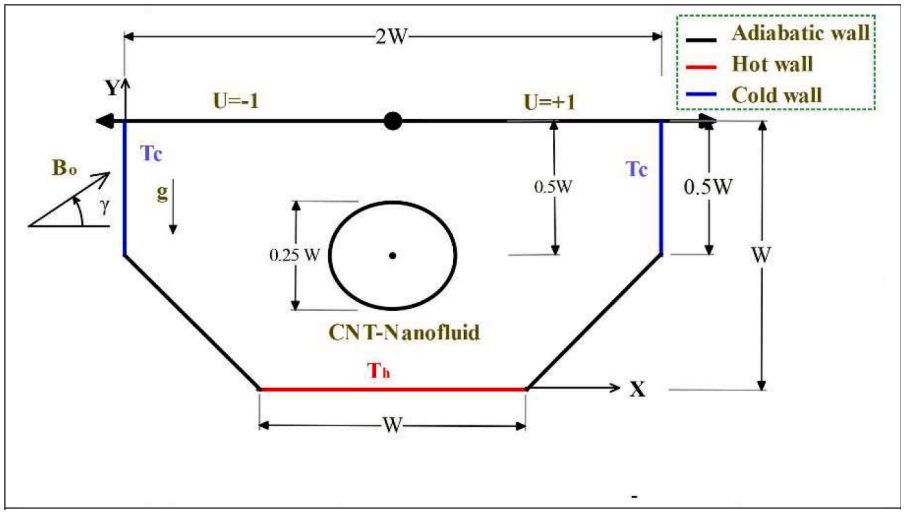

Fig. 1. The geometry.

findings confirmed that heat and fluid flow positively effected by Gr and Ri while negatively effected by *Re*. Different shape enclosure, l-shaped, was numerically studied by Armaghani et al. [25]. Authors searched combined convection under the MHD influence and the hybrid fluid. The aspect ratio of the geometry, according to the results, can highly effect the fluid and heat transformation, where the smallest aspect ratio was the most efficient in enhancing heat and fluid flow. A triangular enclosure with different inner obstacles with moving the top wall were numerically searched by Xiong et al. [26]. They revealed that heat and fluid are both enhanced by rising *Re* while decreased by rising Ri. Colak et al. [27] numerically investigated double convection in an enclosure with chamfer. They tested a range of radius chamfer (0.1 to 0.3) and it was revealed that the chamfer radius can affect fluid flow and heat transfer.

Researchers have found that the fluid streams and heat transformation can be modified using nanoparticles [28,29]. Armaghani et al. [30] numerically searched the effect of adding CuO to the base fluid, water, on the combined convection in a C- enclosure. The influence of the considered nanofluid was tested with considering some important variables such as Ri, *Re* and volume concentration. It was found that heat transfer enhanced with the increase of the volume fraction and the influence of the volume fraction become high at higher Ri number. Zhou et al. [31] numerically examined the influence of using Al_2O_3-water on the mixed convection in 3-D cubical enclosure in which two surfaces were moving. The Nu_{avg} was increased as increasing of ϕ at all Ri values. SiO_2 nanoparticles with different volume concentration were numerically examined Selimefendigil et al. [32]. A range of volume concentration were examined and the results confirmed the previous results, where the transformation enhances with the volume fraction rising. Some different nanoparticles (CuO, Al_2O_3, TiO_2 and Cu) were examined by Loni et al. [33] in order to present the more effective type. These nanoparticles were taken with a wide range of volume concentration, the most effective choice from the thermal prospective was Al_2O_3 while CuO overcome other types from the exergy prospective. Kareem et al. [34] examined the influence of four different types of nanofluids (TiO_2, CuO, SiO_2 and Al_2O_3) on the free forced convection. The findings reveled that the SiO_2 is the most effective nanofluid, where it gave the highest Nu values; on the other hand, CuO had the less influence among the four types. Carbon nanotube has been used widely by many researchers [35–37], where the authors found that this nanfluid is an effective in enhancing heat transfer due to its thermal properties.

Magnetohydrodynamic can highly influence the thermal

Table 1
Base fluid and the exploited nanoparticles (H_2O/CNT) [45].

Material	$\rho\left(\frac{kg}{m^{\wedge 3}}\right)$	k($\frac{W}{m*K}$)	C_p($\frac{J}{kg*K}$)	β ($\frac{1}{K}$)	μ(Pas)
H_2O	997.1	0.6131	4179.1	1.67×10^{-5}	8.9×10^{-4}
CNT	1350	3500	650	4.2×10^{-5}	–

transformation as well as fluid flow and hence it can be a parameter to control those two phenomenon [38–41]. The effect of the MHD on the combined convection in a triangular enclosure was examined by Chamkha et al. [42]. Authors indicated that the trnasormation of heat as well as the fluid flow are highly decreased with the increase of Ha number. Yuan et al. [43] studied the impact of exploiting various strengths of magnetohydrodynamic up on the combined convection in a wavy cavity. A wide range of Ha number was considered from which they concluded that the transformation of heat decreases with the increase of the Ha number. Furthermore, the entropy generation decreases with the increase of the Ha. Bilal et al. [44] numerically examined the impact of using different strengths of MHD field on the natural convection in an enclosure with star shape. The results showed that the convection is decreased as of Ha rise and hence the transformation of heat is declined. important variables that can influence heat enhancement and fluid flow. The current paper aims to investigate the influence of using carbon nanotube nanoparticles on the forced/free convection as well as entropy generation under inclined MHD in a novel geometry in which the top surface is split to move independently to get a motion in different directions. Also, it investigates the influence of using an adiabatic cylinder, in the cavity's core with different sizes, on both flow and transformation of heat. The considered geometry can be used in one of the renewable applications current case can be an application of renewable energy. The study was carried out with different variables such as *Re* (40–200), Ri (0.01–10), Ha (0–62), ϒ (0–60), and ϕ (0–0.08), to understand the influence of these parameters on the heat transfer and fluid flow. Furthermore, the influence of these variables on heat and flow has been presented using contours, diagrams, and tables.

2. Mathematical modeling

2.1. Physical model

The setup of the current geometry is fully described in Fig. 1, which also presents the important boundary conditions (B.Cs). The enclosure is curvilinear with an adiabatic cylinder in the center of the enclosure which is 0.25 W in diameter where W presents a non-dimensional cavity height. The bottom base presents the hot surface, T_h, and its dimension is equal to W. The upper serface is adiabatic and split to drive the flow in to two different directions. vertical walls considered to be cold, T_C, at a fixed velocity. Furthermore, The cavity is filled with CNT nanofluid which explained in Table 1. Moreover, the width of the cavity equals 2 W while the height equals to W.

2.2. Numerical equations

The numerical equations that governed the flow inside the cavity depend on some assumptions like laminar flow, steady flow, and incompressible under the Boussinesq approximation are presented below: [46–48].

$$\frac{\partial u}{\partial x}+\frac{\partial v}{\partial y}=0 \tag{1}$$

$$u\frac{\partial u}{\partial x}+v\frac{\partial u}{\partial y}=-\frac{1}{\rho_{nf}}\frac{\partial p}{\partial x}+\nu_{nf}\left(\frac{\partial^2 u}{\partial x^2}+\frac{\partial^2 u}{\partial y^2}\right)+\frac{\sigma_{nf}B_o^2}{\rho_{nf}}\sin(\gamma)(v\cos(\gamma)-u\sin(\gamma)) \tag{2}$$

$$u\frac{\partial v}{\partial x}+v\frac{\partial v}{\partial y}=-\frac{1}{\rho_{nf}}\frac{\partial p}{\partial y}+\nu_{nf}\left(\frac{\partial^2 v}{\partial x^2}+\frac{\partial^2 v}{\partial y^2}\right)+g\frac{(\rho\beta_T)_{nf}}{\rho_{nf}}(T-T_c)+\frac{\sigma_{nf}B_o^2}{\rho_{nf}}\cos(\gamma)(u\sin(\gamma)-v\cos(\gamma)) \tag{3}$$

$$u\frac{\partial T}{\partial x}+v\frac{\partial T}{\partial y}=\alpha_{nf}\left(\frac{\partial^2 T}{\partial x^2}+\frac{\partial^2 T}{\partial y^2}\right) \tag{4}$$

The dimensionless governing equations can be generated by introducing the following non dimentional parameters:

$$X=\frac{x}{W},\ Y=\frac{y}{W},\ U=\frac{uW}{\alpha_f},\ V=\frac{vW}{\alpha_f},\ \theta=\frac{T-T_l}{(T_h-T_l)},\ P=\frac{pW^2}{\rho_{nf}\alpha_f^2}$$

$$\mathrm{Re}=\frac{U_oW}{\nu_f},\ \mathrm{Gr}=\frac{g\beta_T(T_h-T_c)W^3}{\nu_f^2},\ \mathrm{Ri}=\frac{\mathrm{Gr}}{Re^2},\ \mathrm{Pr}=\frac{\nu_f}{\alpha_f},\ \mathrm{Ha}=B_oW\sqrt{\frac{\sigma_{nf}}{\rho_{nf}\nu_{nf}}},$$

$$\frac{\sigma_{nf}}{\sigma_f}=1+\frac{3\phi\times\left(\frac{\sigma_p}{\sigma_f}-1\right)}{\left(\frac{\sigma_p}{\sigma_f}+2\right)-\phi\times\left(\frac{\sigma_p}{\sigma_f}-1\right)} \tag{9}$$

The Eqs. (2–5),depending on the above non-dimentional parameters, can be written as below: [46–48]:

$$\frac{\partial U}{\partial X}+\frac{\partial V}{\partial Y}=0 \tag{10}$$

$$U\frac{\partial U}{\partial X}+V\frac{\partial U}{\partial Y}=-\frac{\partial P}{\partial X}+\frac{\mu_{nf}}{\rho_{nf}\nu_f}\frac{1}{Re}\left(\frac{\partial^2 U}{\partial X^2}+\frac{\partial^2 U}{\partial Y^2}\right)+\frac{\mathrm{Ha.Ha}}{Re}*\sin(\gamma)(V*\cos(\gamma)-U*\sin(\gamma)) \tag{11}$$

$$U\frac{\partial V}{\partial X}+V\frac{\partial V}{\partial Y}=-\frac{\partial P}{\partial Y}+\frac{\mu_{nf}}{\rho_{nf}\nu_f}\frac{1}{Re}\left(\frac{\partial^2 V}{\partial X^2}+\frac{\partial^2 V}{\partial Y^2}\right)+\frac{(\rho\beta_T)_{nf}}{\rho_{nf}\beta_f}\mathrm{Ri}\theta+\frac{\mathrm{Ha.Ha}}{Re}\cos(\gamma)(U*\cos(\gamma)-V*\sin(\gamma)) \tag{12}$$

$$U\times\frac{\partial\theta}{\partial X}+V\times\frac{\partial\theta}{\partial Y}=\frac{1}{\mathrm{Re}\cdot Pr}\frac{\alpha_{nf}}{\alpha_f}\left(\frac{\partial^2\theta}{\partial X^2}+\frac{\partial^2\theta}{\partial Y^2}\right) \tag{13}$$

2.3. Model presumptions

The thermophysical properties of the nanofluid are obtained depending on the following equations [47,49].

$$\alpha_{nf}=\frac{k_{nf}}{(\rho c_p)_{nf}} \tag{14}$$

$$\rho_{nf}=(1-\phi)\rho_f+\phi\rho_s \tag{15}$$

$$(\rho c_p)_{nf}=(1-\phi)(\rho c_p)_f+\phi(\rho c_p)_s \tag{16}$$

$$(\rho\beta_T)_{nf}=(1-\phi)(\rho\beta_T)_f+\phi(\rho\beta_T)_s \tag{17}$$

$$(\rho\beta_c)_{nf}=(1-\phi)(\rho\beta_c)_f+\phi(\rho\beta_c)_s \tag{18}$$

Thermal conductivity of the nanofluid ca be obtained applying the Maxwellmodel [50]:

$$\frac{k_{\mathrm{nf}}}{k_f}=\frac{k_s+2k_f+2\phi\times(k_s-k_f)}{k_s+2k_f-\phi\times(k_s-k_f)} \tag{19}$$

The local and average Nusselt number for the hot source, i.e. the base of the cavity, is expressed below:

Table 2
Average Nu a longe hot serface with the varying mesh at $Re = 100$, Ri = 10, Ha = 15, ϕ = 0.03.

Mesh element	Nu_{avg}
2527	9.3711
3954	9.3786
11,513	9.3924
30,602	**9.4139**
43,262	9.4135

$$\mathrm{Nu}_{\mathrm{loc}} = -\frac{\partial\theta}{\partial Y} \tag{20}$$

$$\mathrm{Nu}_{\mathrm{avg}} = \frac{1}{W}\int_0^W Nu_{loc}|dY \tag{21}$$

2.4. Boundary conditions

The B.Cs that which have been considered are as following:
At the hot serface: $\theta = 1$, $V = U = 0$
At the top serface: $U = \pm 1, V = 0$, $\mathrm{d}\theta = 0$
At the vertical serfaces: $\theta = 0$, $V = U = 0$
For the cylinder and the inclined walls: $U = 0, V = 0$, $\mathrm{d}\theta = 0$

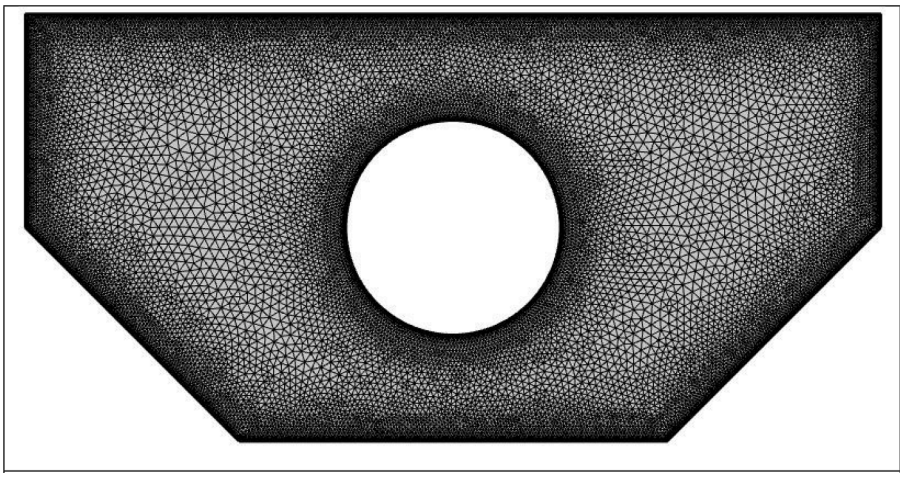

Fig. 2. The mesh type.

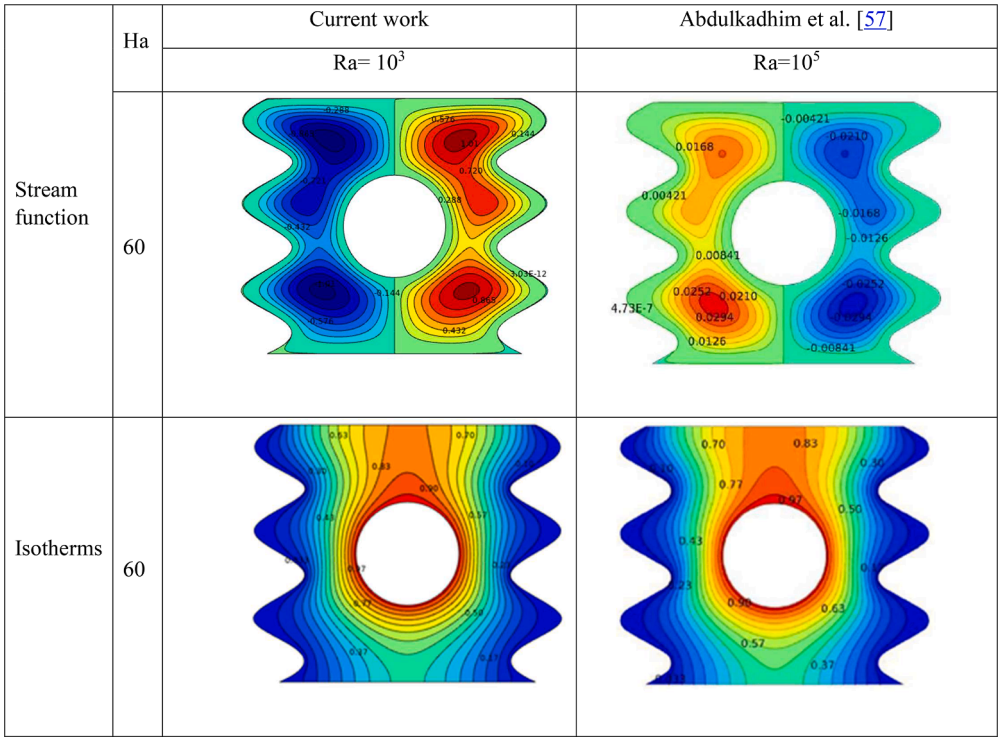

Fig. 3. The stream lines and isotherms of current work with Abdulkhdim [55] at $q = 4$, $\Phi = 0.03$.

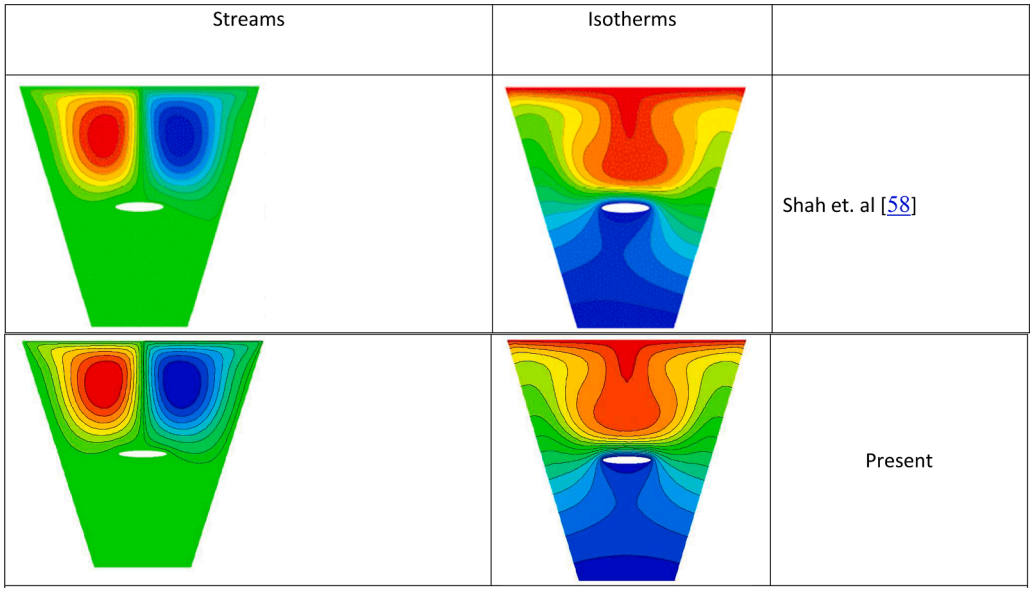

Fig. 4a. Validation with Shah et al. [56] at $Re = 200$, Ri = 0.1, $N = -1$ and Le = 0.1.

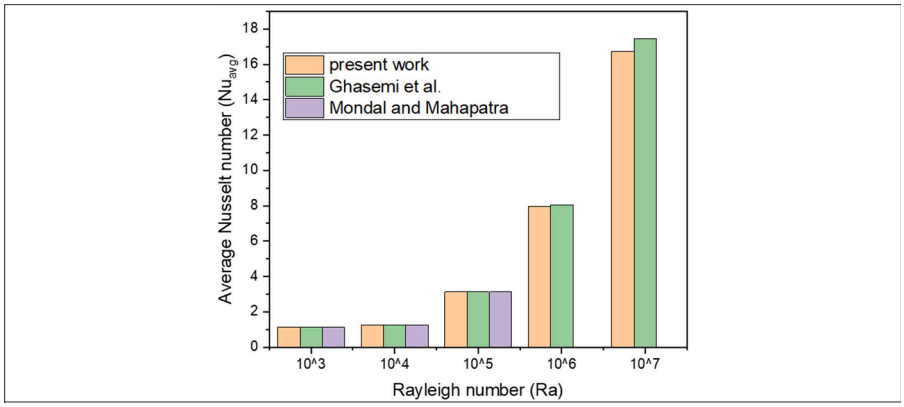

Fig. 4b. Validation with Ghasemi et al. [57] and Mondal and Mahapatra [47] for Ra = 103, Ha = 60, $N = = 0.8$, and φ = 0.03 of Al2O3/water.

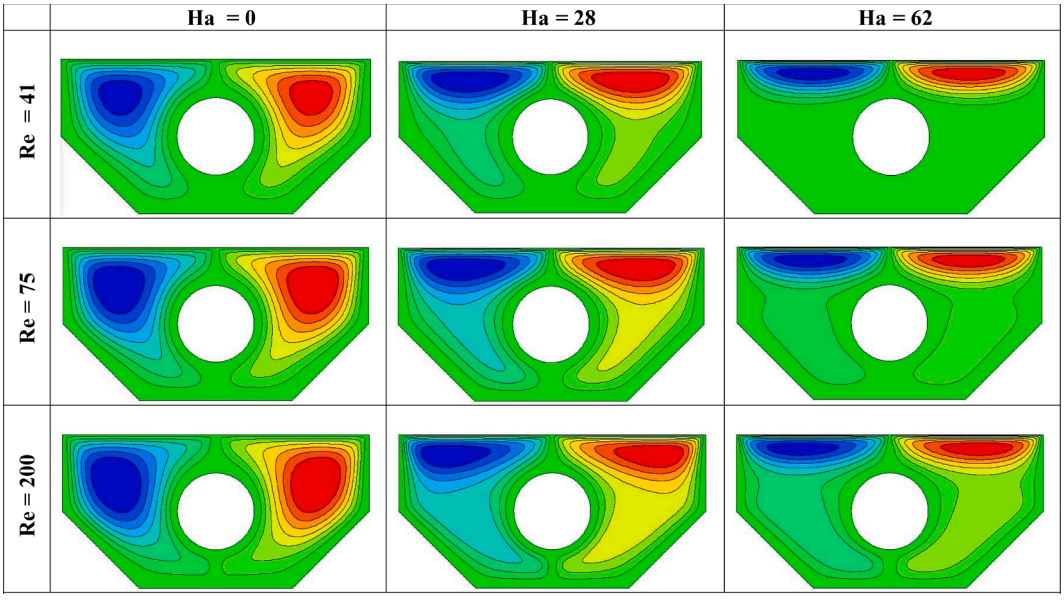

Fig. 5. The contours of Streams with different values of *Re* and Ha at constant values Ri = 7.1, $\gamma = 0$, $\phi = 0.02$.

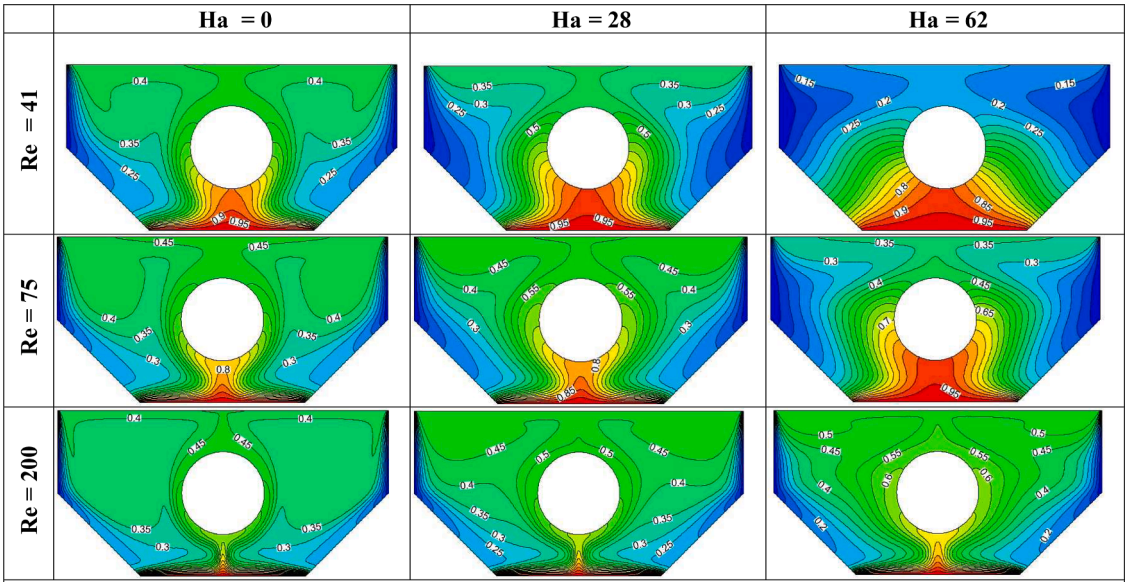

Fig. 6. The contours of isotherms with different values of *Re* and Ha at constant values of Ri = 3, $\gamma = 0$, $\phi = 0.01$.

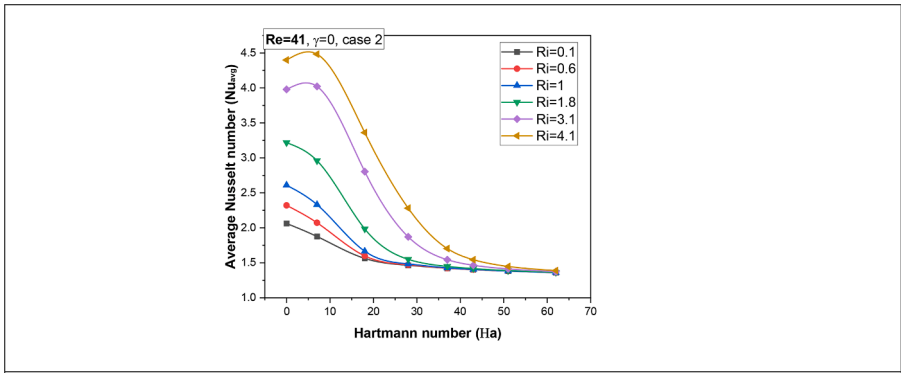

Fig. 7. The variation Average Nusselt number with different values of Ha and Ri numbers and constant *Re* = 41, $\gamma = 0$, $\phi = 0.01$.

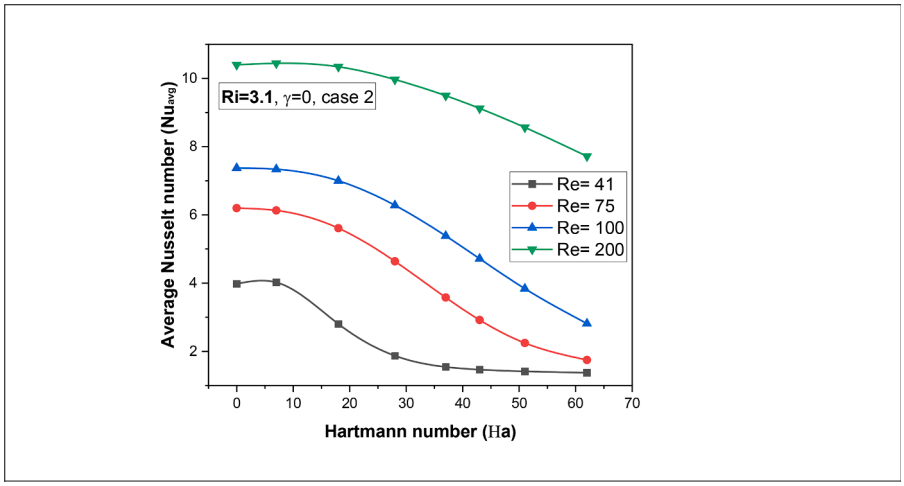

Fig. 8. The variation Average Nusselt number with different values of Ha and *Re* at constant Ri = 3.1, $\gamma = 0$, $\phi = 0.01$.

2.5. Entropy generation

The irreversibilities are responsible for the entropy which are generated because of heat transfer, S_{HT}, the flow of fluid, S_{FF}, and the magnetohydrodynamic, S_{MG}. These types of entropy can be presented as [51,52]:

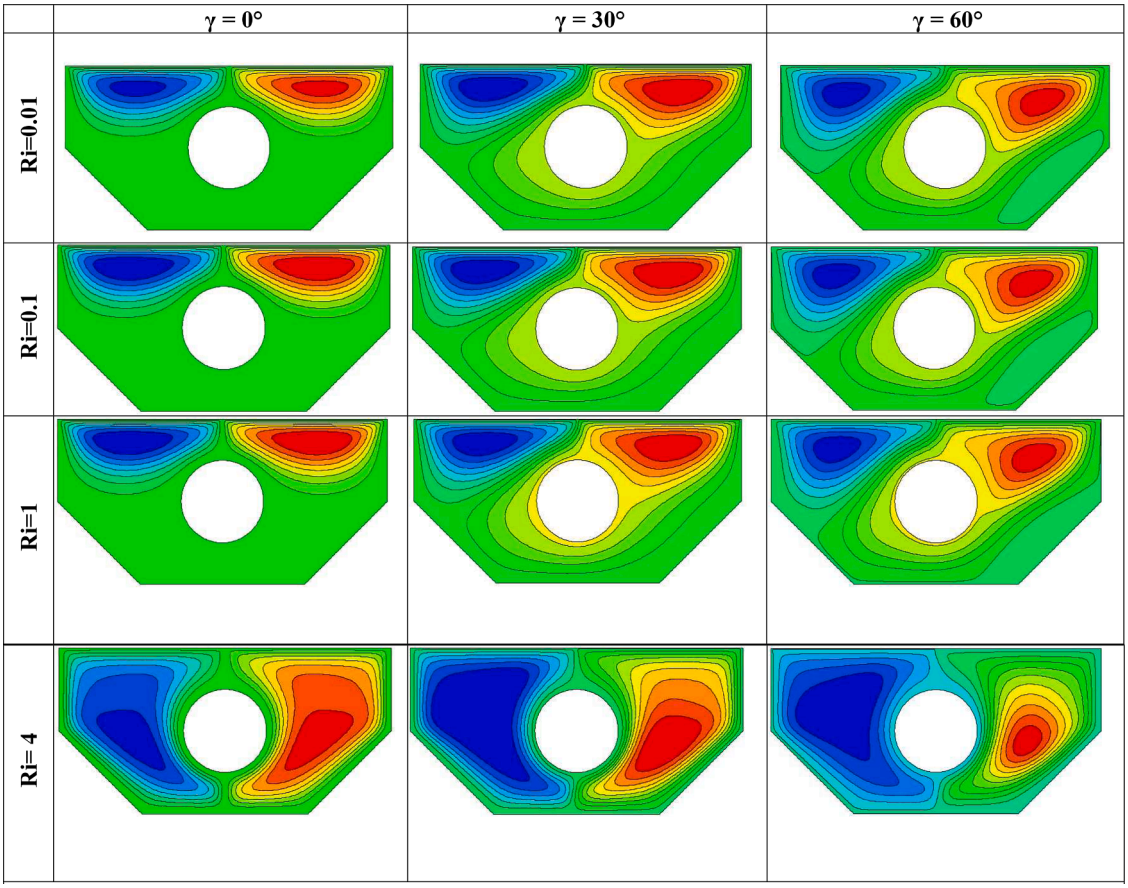

Fig. 9. The contours of Streams with different values of Ri and γ at constant values of Ha = 60 and ϕ = 0.01.

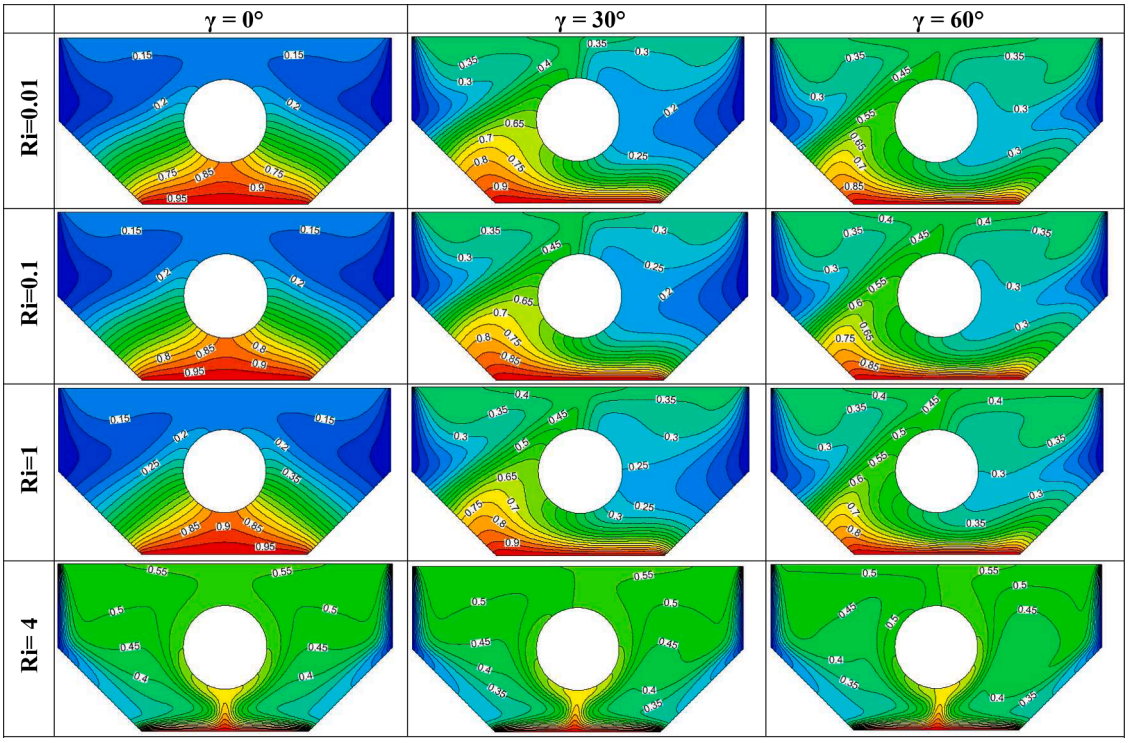

Fig. 10. The contours of isotherms with different values of γ and Ri at constant values of Ha = 60 and ϕ = 0.01.

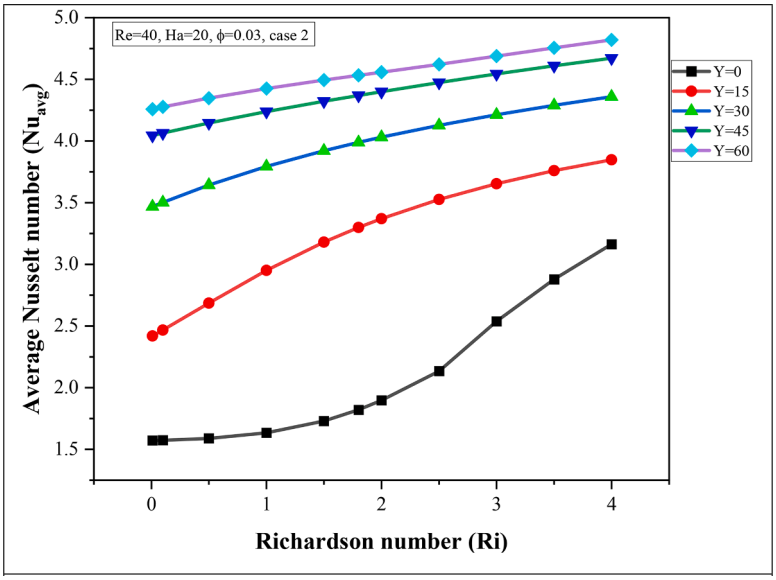

Fig. 11. The variation Average Nusselt number with different values of Ri and γ at fixed values of Ha = 20, *Re* = 40, ϕ = 0.03.

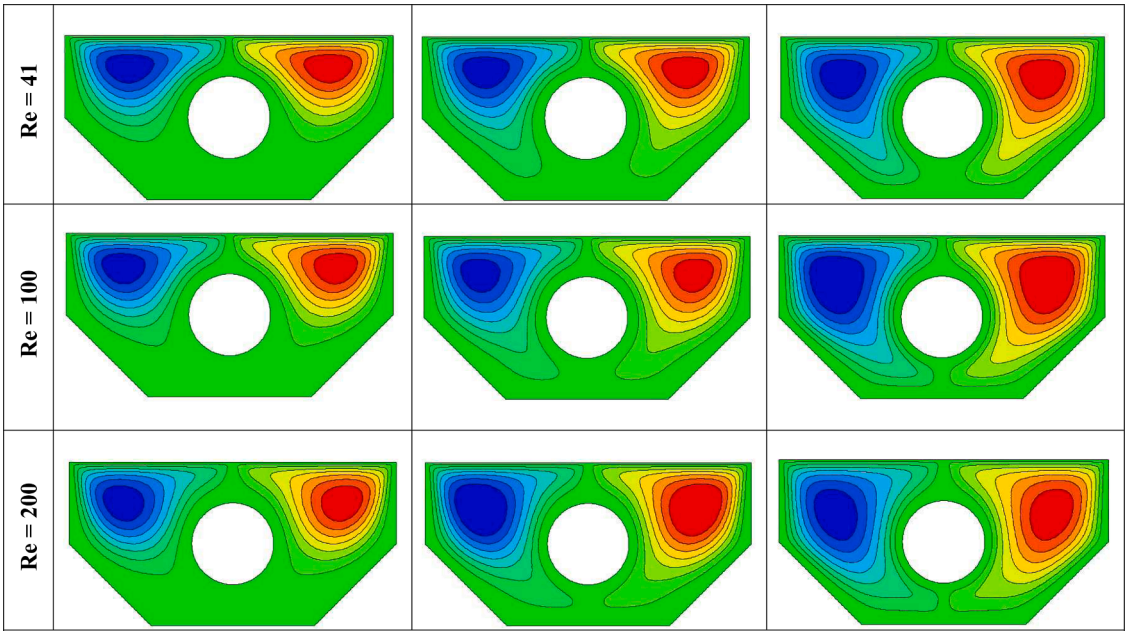

Fig. 12. The contours of Streams with different values of *Re* and Ri at constant Ha = 15, ϕ = 0.01 and γ = *0*.

$$S_{HT} = \lambda_1\left(\frac{\mu_{nf}}{\mu_f}\right)\left[\left(2\left(\frac{\partial u}{\partial x}\right)^2+\left(\frac{\partial v}{\partial y}\right)^2\right)+\left(\left(\frac{\partial u}{\partial y}\right)^2+\left(\frac{\partial v}{\partial x}\right)^2\right)\right] \quad (22)$$

$$S_{FF} = \left(\frac{k_{nf}}{k_f}\right)\left(\left(\frac{\partial T}{\partial x}\right)^2+\left(\frac{\partial T}{\partial y}\right)^2\right) \quad (23)$$

$$S_{MG} = \lambda_1\left(\frac{\mu_{nf}}{\mu_f}\right) Ha^2.U^2 \quad (24)$$

The entropy generation from all irreversibilities equals the summation of equation (27–30)

$$S_{total} = S_{HT} + S_{FF} + S_{MG} \quad (25)$$

The value of λ_1

$$\lambda_1 = \frac{\mu_f}{k_f}.\left(\frac{T_h+T_c}{2}\right).\left(\frac{U_o}{T_h+T_c}\right)^2, \quad (26)$$

The value for λ_1 is taken as 0.0001 [53,54]

3. Numerical study

The Finite Element Method, FEM, is the numerical method which has been considered to model the variables. The Galeerkin technique is used in the current work with non-uniform triangular mesh. Near the solid surfaces, there is an important physical change that needs highly refined mesh to be captured. However, the domine away from the solid surfaces dose not require high refine mesh for that reason is very important to consider a local refinement by which a fewer mesh elements would be used. The convergence method which should be reached by all the non-dimensional variables (P, U, V, θ) using the iteration is:

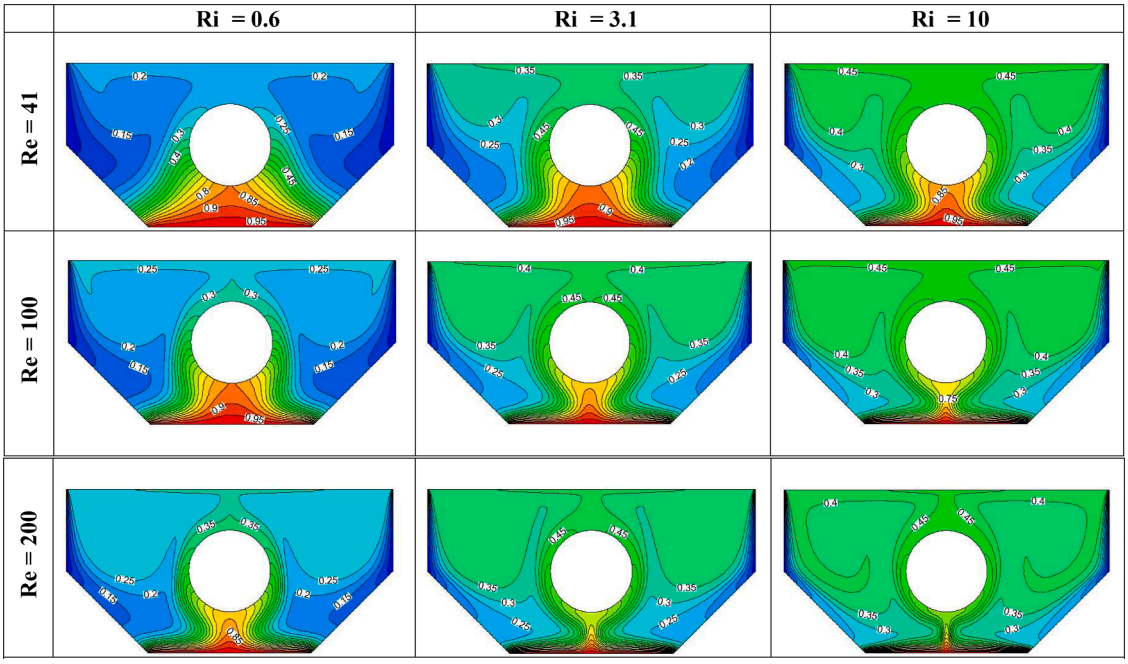

Fig. 13. The contours of isotherms with different values of *Re* and Ri at constant values of Ha = 15, ϕ = 0.01 $\gamma = 0$.

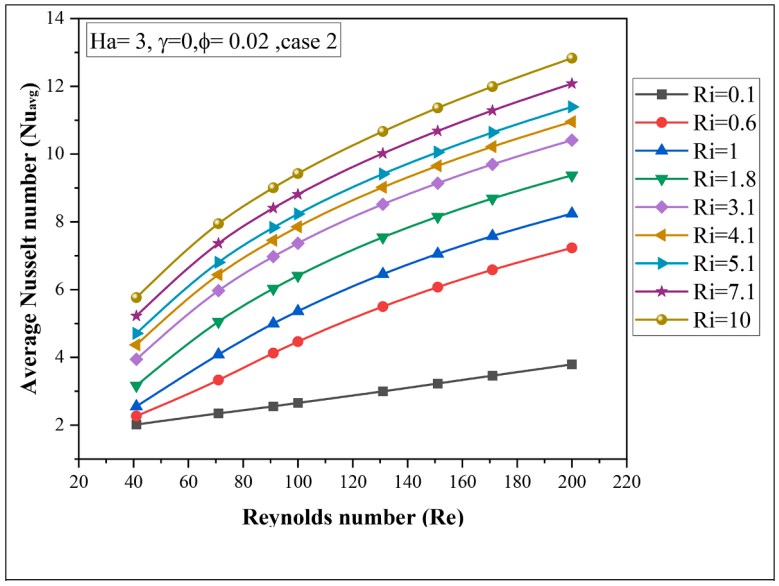

Fig. 14. The variation Average Nusselt number with different values of *Re* and Ri at fixed values of Ha = 3, γ = 0 and ϕ = 0.02.

$$\left|\frac{\xi^{i+1}-\xi^{i}}{\xi^{i+1}}\right| \le 10^{-5}$$

The accuracy of the numerical results is highly affected by the type of the mesh as well as the number of elements. To be sure that the appropriate type of mesh has been used, a mesh dependency study must be done before making the numerical analysis. This is the reason for doing the mesh independency, as can be seen in Table 2, which indicates that grid 4 is the most accepted grid with fewer elements as can be seen in Fig. 2.

4. Model validation

After the mesh dependency study, the current model must be validated with previously published papers to be sure that the model has been set correctly. For that reason, a validation study with two published papers has been made as can be seen in Fig. 3 and 4. Where Fig. 3 explains a validation of the current paper with Abdulkhdim et al. [55]. at different values of Ra number and Ha number and fixed values of heat generation, $q = 4$, and volume concentration, $\Phi = 0.03$. The isotherms of the current paper and the published paper are very similar, this means that modelling the nanofluid is correctly coded. Another validation has been done with Shah et al. [56] at *Re* = 200, Ri = 0.1, *N*= -1 and Le = 0.1 as can be seen in Fig. 4a. where both isotherms and streams are drawn with the current paper.

To confirm the accuracy of the current code, another validation with two published papers has been explained in (Fig. 4b) for different Ra numbers and fixed values for other parameters such as Ha = 30 and Φ = 0.04. The values of Nu_{avg} for the current paper and the published papers are very similar and hence confirm the accuracy of the current code.

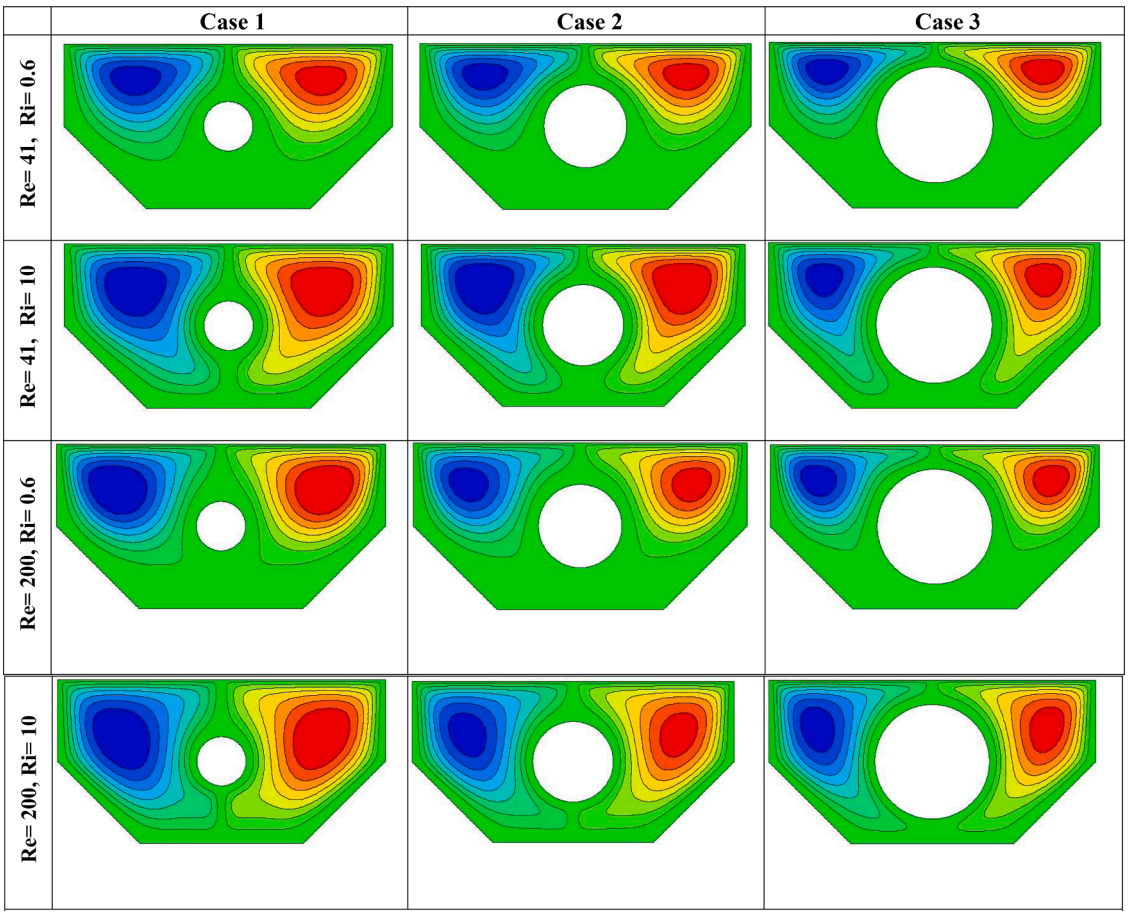

Fig. 15. The contours of Streamlines with different values of *Re* and Ri and different cases at constant values of Ha = 0, ϕ = 0.01.

5. Results and discussion

The present work numerically searched the influence of applying MHD in different angles and the entropy generation on combined convection in an enclosure in which the top serface split to make a two lid-drives and an adiabatic cylinder. Furthermore, a special type of nanoparticle, carbon nanotube, has been added to the base fluid, water with constant Pr number (Pr=6.2), in different concentrations to investigate its influence on the flow and heat transfer. Moreover, some other parameters that have been considered were *Re* (41 - 200), Ri (0.01–10), Ha (0–62), ɣ (0–60o), and ϕ (0–0.06).

5.1. Influence of magntohydrodynimic and the inclination angle

Fig. 5 shows how the MHD influences the flow of the fluid at different strengths (Ha = 0, 28, 62) and different *Re* (*Re* = 41, 75, 200) while fixing other variables such as Ri (Ri = 7.1), ɣ (ɣ = 0) and ϕ (ϕ = 0.02). From the contours, at low *Re* and free MHD, the flow of fluid spread in the cavity with two strong vortices in different directions mainly concentrated near the lid drives. As the force of MHD is present, the streams are minimized in the main cavity and concentrated close to the lid drives. The reason behind that is the force of Lorentz which is supplied along the x-axis and depending on the right-hand rule, it acts vertically to force the streams to the up. Furthermore, the streams totally concentrated on the top are at high MHD. As the *Re* number increases, the influence of the streams circulates strongly and distributed in the cavity, however, the force of the MHD pushes most of the streams to the top are with fewer streams around the cylinder.

Fig. 6 explains the influence of the Magnetic field on the isotherms contours for different Ha (0, 28, 62) and different *Re* (41, 75, 200) with constant Ri (Ri = 3), (ɣ = 0), (ϕ = 0.01). The influence of MHD on isothermals is noticeable with low *Re* number, *Re* = 41, where the isothermals are distributed from the bottom to the upper serface at free MHD. Moreover, as Ha rises the isotherms are distributed in the bottom region. This behavior of isothermals is due to having less flow circulation with the presence of the MHD and hence the isothermals depend only on the bouncy in spreading throughout the cavity. Furthermore, as *Re* rises, the flow circulation increases with less effect by the presence of the MHD; consequently, the isotherms spread through the cavity even with the high presence of the MHD.

For more explanation of the influence of MHD on heat transfer, Fig. (7) presents the influence of applying different values of Ri number with a range of Ha number on the value of average Nu at constant *Re* (*Re* = 41), ɣ (ɣ = 0) and case 2. The convection declines as Ha rise for all Ri values; however, the influence of the Ha number increases with the increase of the Ri number. Fig. 8 presents the impact of Ha number on the average Nu with a range of *Re* (41, 75, 100, and 200) and constant Ri (Ri = 3.1), ɣ (ɣ = 0), and case 2. For all values of the *Re*, the increase of Ha results in droping the values of the average Nu number; however, the influence of MHD is less with a high *Re* number. This is because of high circulation with a high *Re* number with a very high Ha number; hence, the flow streams push the isotherms throughout the cavity and this increases the convection.

On the other hand, when the orientation of the MHD changes, changing the inclination angle of the MHD, there is a new trend for the MHD. Fig. 9 presents the impact of the inclination angle on the streams at different inclination angles (0, 30, 60) and Ri number (0.01, 0.1, 1, 4) at Ha= 60, ϕ = 0.01, and case 2. It is clear that with the increase of the inclination angle, the influence of the MHD changes with the angle according to the right-hand rule. Furthermore, instead of compressing the

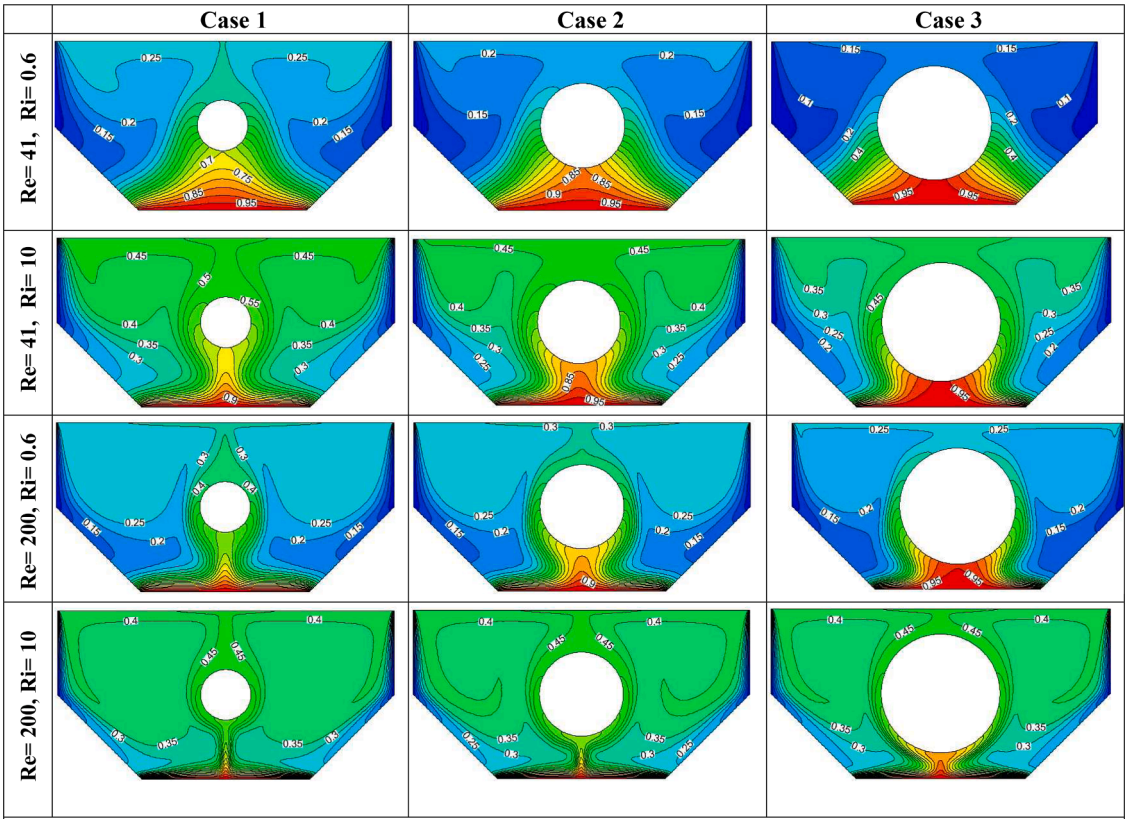

Fig. 16. The contours of isotherms with different values of *Re* and Ri and different cases at constant values of Ha = 0, ϕ = 0.01.

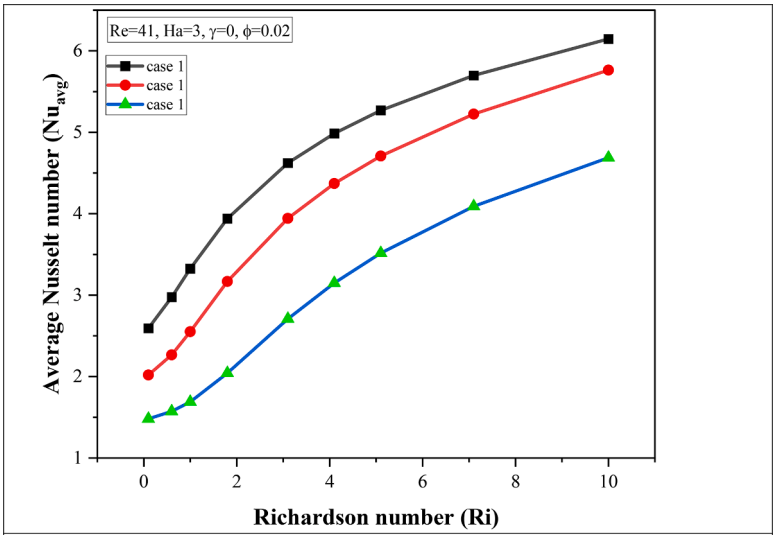

Fig. 17. The variation Average Nusselt number with different cases at *Re* = 41, Ha = 3, ϕ = 0.01.

streams to the top region at ($\gamma = 0$), the magnetic field at ($\gamma = 30$) pushes the streams of the right vortices through the geometry. Furthermore, at ($\gamma = 60$), the influence of the MHD includes both vortices, and hence the streams are more streams are pushed from the top area to the cavity. This behavior of the streams has a great influence on the isotherms as can seen in Fig. 10, where these streams that have been moved from the top to the down of the cavity can push the isotherms away from the hot surface. This behavior is very effective at low Ri numbers and less effective with high Ri numbers. This trend is more explained in Fig. (11), which explians the variation of average Nu with a range of inclination angle and Ri, where the value of Nu_{avg} increases as the inclination angle increase. Also, the influence of the inclination angle on the Nuavg is higher for low Ri number.

5.2. *The influence of Reynolds and Richardson number*

The influence of *Re* number and Ri number on streams and isotherms is well presented in Figs. 12 & 13 with a range of *Re* (41, 100, 200) and Ri (0.6, 3.1, 10) at constant Ha (Ha = 15), ϕ (ϕ = 0.01) and case 2. It is clear from Fig. 12 that the streams are highly influenced by the change of the Ri number at all *Re* values. However, the influence of the *Re* number depends on the value of the Ri number, where *Re* influence is

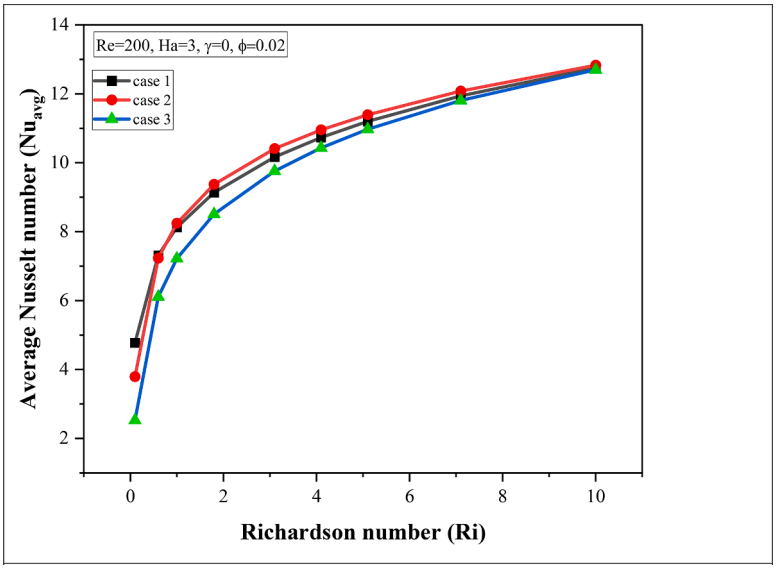

Fig. 18. The variation Average Nusselt number with different values with different cases at fixed values of $Re = 200$, Ha = 3 and $\phi = 0.01$.

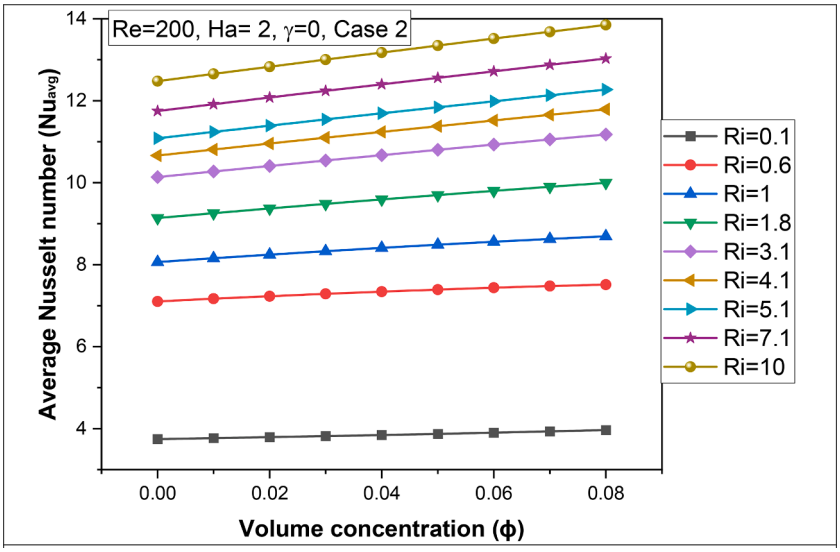

Fig. 19. The variation Average Nusselt number with different values of Ri and ϕ at constant values of $Re = 200$, Ha = 2 $\gamma = 0$.

only sensible when the value of the Ri number is high.

On the other hand, Fig. 13 explains that the isotherms are highly influenced by both *Re* and Ri. At constant *Re*, the rise of Ri increases the distribution of isothermals because of rising the bouncy force which drive the isothermls to the top area. Furthermore, the strength of isotherms becomes at its higher level with high values of Ri and *Re*. Moreover, at constant Ri number, the isotherms are also noticeably influenced by changing *Re* number.

The enhancement of heat transformation can be well understood from the chart of average Nu numbers with a range of *Re* and Ri numbers, Fig. 14. It is clear that increasing the Ri number enhances the transformation of heat for all values of the *Re* number. However, the influence of Ri number on heat transfer increases with the increase of *Re* number to be at a maximum influence at maximum *Re*. On the other hand, the increase of the *Re* number enhances the transformation of heat for all the Ri values and its influence becomes maximum at high Ri number.

5.3. *Impact of the cylinder's size and volume concentration*

The influence of the adiabatic cylinder on the streams and isotherms contour is well presented in Figs. (15 & 16), where three different sizes are tested with a range of Ri (0.6, 10) and *Re* (41,10) at constant other variables. From Fig. 15, it is clear that the influence of the cylinder's size is effective at low *Re* (41) and Ri (0.6), where the circulation of the flow is very weak and the cylinder acts as an obstacle in the flow path. As the *Re* increases the influence of the size becomes less because the streams flow around the obstacle with the same strength for all cases. On the other hand, the isotherm contour, as can be seen in Fig. 16, presents the same trend, where the influence of the cylinder is only active with low *Re* and Ri numbers.

Fig. 17 explians the variation of the Nu_{avg} with the different cases and a range of Ri number at very low *Re* ($Re = 41$), Ha (Ha = 3), γ ($\gamma = 0$), ϕ ($\phi = 0.02$). It can be seen that the transfer of heat is enhanced with the decrease of the cylinder for all values of the Ri number. In contrast with Fig. 18 in which a high *Re* number has the experience, $Re = 200$, it can be seen that the transfer of heat for the three cases is nearly similar.

Table 3
Average Nusselt number at different values of *Re* and Ri and constant values of Ha = 3, ϕ = 0.02 and ɣ = 0.

		Re = 41	*Re* = 71	*Re* = 91	*Re* = 100	*Re* = 131	*Re* = 151	*Re* = 171	*Re* = 200
Case 1	Ri	Nuavg							
	0.1	2.5937	3.1053	3.4151	3.5496	3.9895	4.2469	4.4809	4.7735
	0.6	2.9757	4.1889	4.9201	5.2126	6.0577	6.4978	6.87	7.3156
	1	3.3252	4.8341	5.6235	5.9281	6.8004	7.2541	7.6452	8.1271
	1.8	3.9393	5.6343	6.4464	6.7592	7.6681	8.1551	8.5867	9.1374
	3.1	4.6226	6.3755	7.2108	7.5375	8.509	9.0451	9.5306	10.166
	4.1	4.9853	6.7577	7.6128	7.9504	8.9652	9.5322	10.05	10.734
	5.1	5.2687	7.0596	7.9346	8.2824	9.3356	9.9292	10.474	11.199
	7.1	5.6985	7.5283	8.4406	8.8065	9.925	10.562	11.151	11.939
	10	6.1474	8.0349	8.9944	9.3821	10.576	11.262	11.898	12.754
Case 2	0.1	2.0197	2.3479	2.5576	2.6537	2.9982	3.2277	3.4616	3.7928
	0.6	2.2673	3.3339	4.1286	4.466	5.4999	6.0726	6.5835	7.23
	1	2.5524	4.0823	4.9971	5.3643	6.46	7.0557	7.582	8.2449
	1.8	3.1683	5.0548	6.0284	6.4125	7.5441	8.1524	8.6895	9.3709
	3.1	3.9436	5.9695	6.9741	7.3671	8.5199	9.1419	9.696	10.409
	4.1	4.3707	6.4391	7.4558	7.8527	9.0191	9.6522	10.22	10.955
	5.1	4.7081	6.8056	7.8312	8.2316	9.4118	10.056	10.636	11.392
	7.1	5.2237	7.3625	8.4031	8.8103	10.018	10.683	11.286	12.078
	10	5.7642	7.9449	9.0053	9.4223	10.668	11.361	11.993	12.829
Case 3	0.1	1.4812	1.6458	1.745	1.7903	1.9609	2.0922	2.2479	2.5248
	0.6	1.5727	2.1439	2.7934	3.1174	4.198	4.8188	5.3811	6.1113
	1	1.6899	2.7705	3.6832	4.073	5.2394	5.883	6.4631	7.221
	1.8	2.0423	3.7875	4.8124	5.9512	6.4241	7.0917	7.7011	8.5095
	3.1	2.7081	5.4762	5.8509	7.1844	7.5194	8.2278	8.8825	9.7582
	4.1	3.1495	6.1377	6.3816	7.7376	8.098	8.8355	9.5191	10.431
	5.1	3.5171	6.6027	6.799	8.1519	8.563	9.326	10.033	10.971
	7.1	4.0901	7.2585	7.4452	8.7724	9.2967	10.099	10.838	11.809
	10	4.688	7.9079	8.1429	9.419	10.097	10.937	11.701	12.699

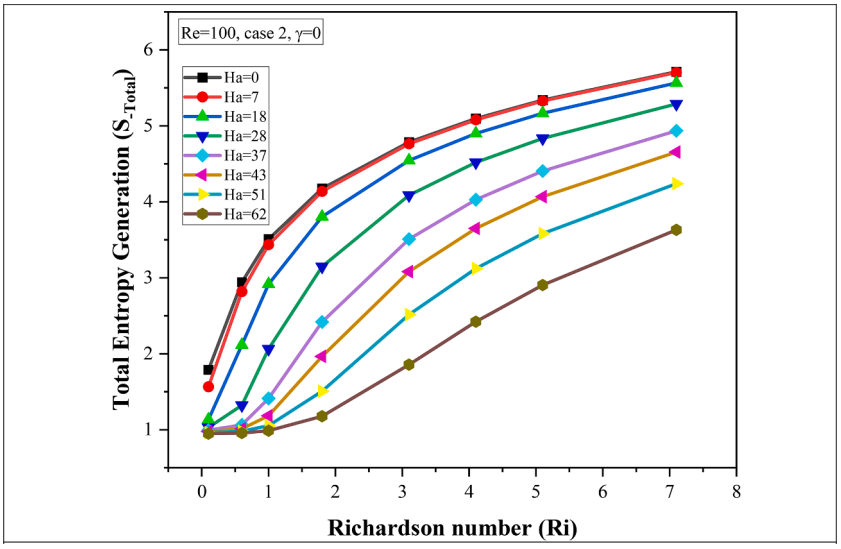

Fig. 20. The variation of total entropy generation with different values of Ha and Ri at constant values of *Re* = 100, case2 and ɣ = 0.

Heat transformation seems to be enhanced by adding nanoparticles to the base fluid. Fig. 19 explains the importance of adding nanoparticles in different concentrations to the transformation of heat at various Ri with constant *Re* (*Re* = 200), Ha (2), case 2, and ɣ (ɣ = 0). The value of Nuavg increases with increase rise of the volume concentration for all the Ri values. However, the influence of the nanoparticles of the transformation of heat enhances with the rise of the Ri to reveal a maximum influence at a higher Ri (Ri = 10). More explanation about the influence of the cylinder's size with a range of data which are *Re* and Ri is explained in Table 3. Furthermore, the highest values of Nu avgare presented for case 3, while the lowest are shown in case 1.

5.4. The influence of entropy generation

Fig. 20 explains the influence of Ri and Ha on the total entropy generation at constant *Re* (*Re* = 100) and ɣ (ɣ = 0). It is clear that the irreversibility highly increases with the increase of the Ri number because of the increase of heat transfer. However, the increase of the MHD decreases the generation of entropy because it increases the transformation of heat transfer. Fig. 21 presents the variation of total entropy generation and *Re* number with a range of Ha number at constant Ri (Ri = 7.1), ɣ (ɣ = 0), and case 2. It is clear that the value of total entropy generation is enhanced with the increase of *Re* for all values of Ha. This means that the irreversibility from fluid flow increases with the increase of the fluid flow. In contrast, at a fixed *Re* number, the value of total entropy generation decreases with the increase of Ha number. On

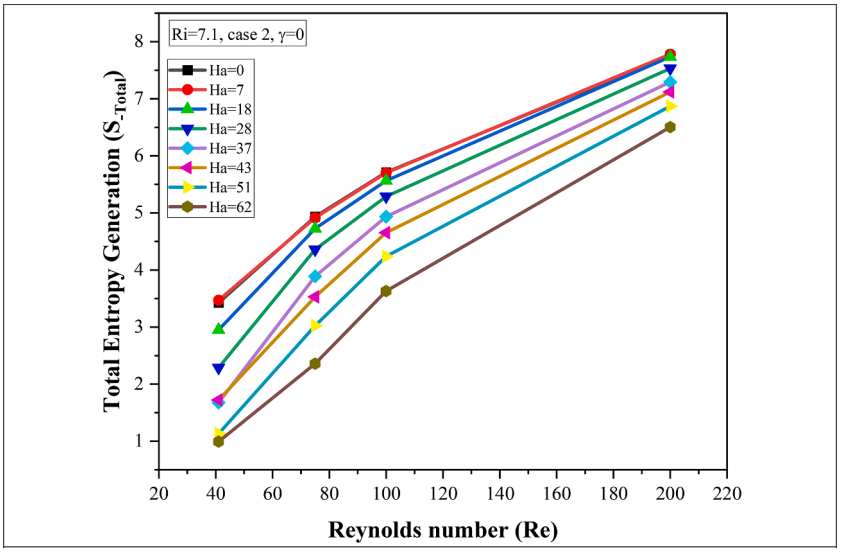

Fig. 21. The variation of total entropy generation with different values of with different values of Ha and *Re* at constant values of Ri = 7.1, case2 and $\gamma = 0$.

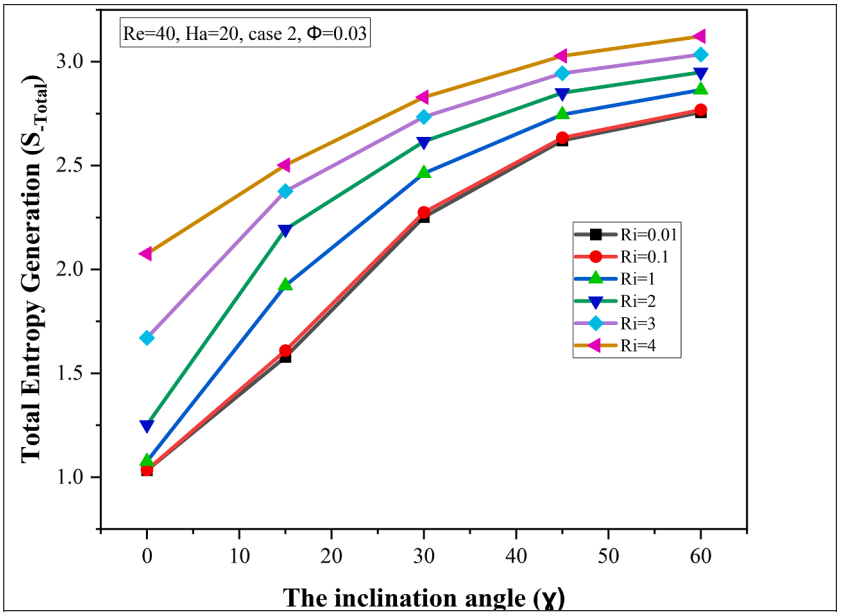

Fig. 22. The variation of total entropy generation with different values of the inclination angle and Ri number at constant values of *Re* = 40, case2 and $\phi = 0.03$.

the other hand, as the orientation of the MHD changes, the entropy generation increases and this increase rises with the increase of the inclination angle as presented in Fig. 22. This is due to the fact that with an inclination angle both the flow streams as well as the transformation of heat are enhanced and this increases the irreversibilities. Fig. 23 explains the influence of entropy generation with the volume concentration with different values of *Re* and Ri while constant Ha (Ha = 3), γ ($\gamma = 0$), and case 2. It can be seen that for low *Re* and Ri, the influence of volume concentration on the entropy generation is not sensible and this is due to less increase in heat transfer at these low values; however, the entropy generation becomes clear at high *Re* and Ri. Fig. 24 explains the influence of cylinder size on the entropy generation at different *Re* and constant Ha (Ha = 3), Ri (Ri = 3), ϕ ($\phi = 0.02$), and γ ($\gamma = 0$). It is observed that increasing the size of the cylinder increases the irreversibilities and this is only sensible with a high *Re* number.

6. Conclusion

The current work studied the influence of inclined magnetohydrodynamics upon forced/free convection as well as the reproduction of entropy in a cavity filled with nanofluid and its lid drive split to give motion in different directions. A range of effective variables has been considered and numerically solved after making a validation for the code which gives an acceptable and good agreement with some published papers. The main points that can be concluded are:

- The transfer of heat as well as the flow of the fluid are greatly influenced by changing Reynolds and Richardson numbers. The remarkable point is that at lower value of Richardson number, the streamlines are fundamentally in the upper area making two vortices which are circulated in opposite directions for all values of *Re*. However, the streams expand to the cavity around the adiabatic cylinder at a high Ri number.

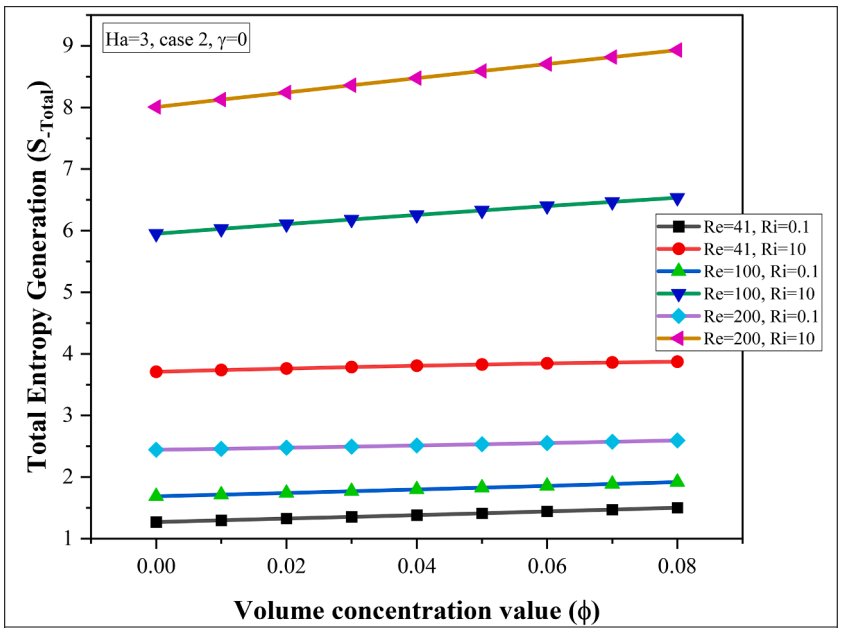

Fig. 23. The variation of total entropy generation with different values of Ri and *Re* at constant values of Ha = 3, case2 and $\gamma = 0$.

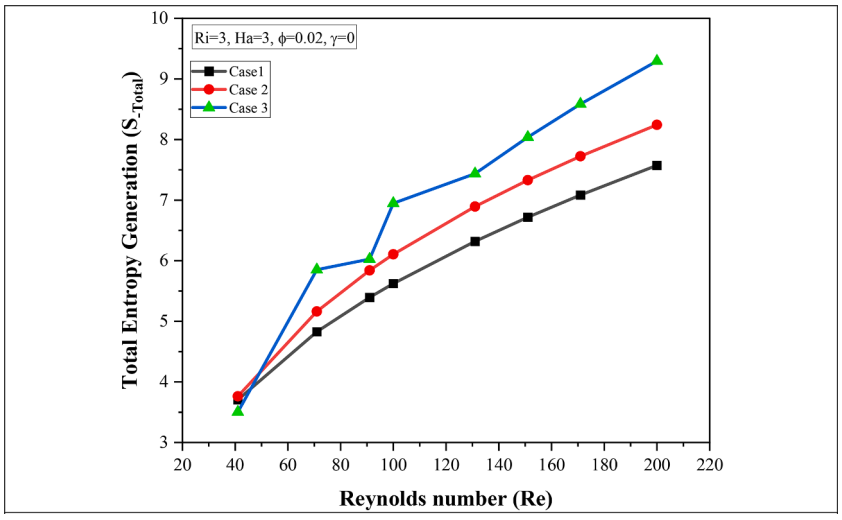

Fig. 24. The variation of total entropy generation with different values of *Re* and different cases at constant values of Ri = 100, $\phi = 0.02$ and $\gamma = 0$.

- The MHD acts to decrease the flow of the streams and compress the flow close to the top of the cavity. Furthermore, the value of Nu_{avg} drops with the rise of the MHD at all the Reynolds and Richardson values. Furthermore, the value of Nu_{avg} decreses by 34.7 % when increasing Ha from 0 to 62 at $Re = 200$. however, as the value of the inclination angle increases the influence of the MHD changes according to the right hand and this increases the flow of the fluid and enhances the transfer of heat.
- Adding nanoparticles increases the transformation of heat, where the value of average Nu increases with the increase of the volume concentration; however, the influence of the nanoparticles is only sensible at high *Re* and Ri numbers.
- The total entropy generation increases with the increase of the Richardson, Reynolds, and volume concentration; however, it decreases with the increase of the MHD. Furthermore, the inclination angle also increases the irreversible and this is because of increasing heat and flow with the inclination angle.
- The best geometry for the heat enhancement is case 2 which gives the higher values of Nusselt average.
- Heat transfer enhances by 57 % when increasing Ri from 0.1 to 10 at $Re = 41$ and this enhancement increases to 62.5 % at $Re = 200$.

7. Future work

7.1. Recommendations

- The recommendations for future work are:
- To explore more than one nanofluid to investigate the most effective type for heat enhancement.
- It is recommended to investigate the current case in different applications and different geometries.
- In many engineering applications that include high heat transfer, there is a radiation factor, this could be added to future work.
- Mass transfer is very recommended to be investigated with heat transfer.

7.2. The advantages, disadvantages, and limitations

The considered model is the Finite element method which is very recommended for the current case and similar cases in which the Ra number ranges from 10^3 to 10^6. there is no problem with the convergence as long as the Ra number is limited. However, if the author wanted to explore a higher number of Ra numbers, especially with some vital parameters such as porous media, and exothermic chemical reactions, then the coverage of such cases would be a big challenge.

CRediT authorship contribution statement

Mohammed Azeez Alomari: Writing – original draft, Validation, Software. **Qusay H. Al-Salami:** Writing – review & editing. **Farah Q. A. Alyousuf:** Formal analysis. **Faris Alqurashi:** Resources. **Mujtaba A. Flayyih:** Project administration.

Declaration of competing interest

The authors declare that they have no known competing financial interests or personal relationships that could have appeared to influence the work reported in this paper.

References

[1] R. Andrzejczyk, T. Muszynski, Thermodynamic and geometrical characteristics of mixed convection heat transfer in the shell and coil tube heat exchanger with baffles, Appl. Therm. Eng. 121 (2017) 115–125.
[2] R. Andrzejczyk, T. Muszynski, An experimental investigation on the effect of new continuous core-baffle geometry on the mixed convection heat transfer in shell and coil heat exchanger, Appl. Therm. Eng. 136 (2018) 237–251.
[3] S. Islam, et al., Numerical investigation with sensitivity study of MHD mixed convective hexagonal heat exchanger using TiO2–H2O nanofluid, Results Eng. 18 (2023) 101136.
[4] S.T. Keya, et al., Mixed convection heat transfer in a lid-driven enclosure with a double-pipe heat exchanger, Int. J. Thermofluids 13 (2022) 100131.
[5] M. Camci, et al., An experimental study on the heat transfer characteristics over a radiant cooled wall exposed to mixed and forced convection driven by displacement ventilation, Int. Commun. Heat Mass Transf. 135 (2022) 106122.
[6] T. Yamamoto, et al., Thermal environment analysis for the optimal operation of combined convection and radiant air conditioning considering dehumidification, Heliyon (2023) e18092.
[7] M. Hadavand, et al., A numerical investigation on the effects of mixed convection of Ag-water nanofluid inside a sim-circular lid-driven cavity on the temperature of an electronic silicon chip, Appl. Therm. Eng. 162 (2019) 114298.
[8] L. Boutina, R. Bessaïh, Numerical simulation of mixed convection air-cooling of electronic components mounted in an inclined channel, Appl. Therm. Eng. 31 (11) (2011) 2052–2062.
[9] D.-H. Shin, et al., Experimental analysis on mixed convection in reactor cavity cooling system of HTGR for hydrogen production, Int. J. Hydrogen Energy 42 (34) (2017) 22046–22053.
[10] L. Liu, et al., Experimental investigation of flow and convective heat transfer on a high-Prandtl-number fluid through the nuclear reactor pebble bed core, Appl. Therm. Eng. 145 (2018) 48–57.
[11] C. Dong, et al., Heat transfer of air turbulent mixed convection in the passive containment air-cooling system of a modular small nuclear reactor, Int. J. Therm. Sci. 182 (2022) 107793.
[12] A. Abdelmaksoud, H.F. Elbakhshawangy, O.S. Abd El-Kawi, Heat transport and chimney design in a typical MTR reactor during natural convection cooling regime, Progr. Nucl. Energy 138 (2021) 103814.
[13] C. Xiao, et al., Numerical investigation of laminar mixed convection of microalgae slurry flowing in a solar collector, Appl. Therm. Eng. 175 (2020) 115366.
[14] T. Long, et al., Experimental study on liquid desiccant regeneration performance of solar still and natural convective regenerators with/without mixed convection effect generated by solar chimney, Energy 239 (2022) 121919.
[15] B. Krittacom, S. Bunchan, R. Luampon, Heat transfer enhancement of solar collector by placing wire mesh stainless porous material on the solar absorber plate of indirect forced convection solar dryer, Therm. Sci. Eng. Progr. 32 (2022) 101304.
[16] M. Ammar, et al., Parametric investigation on the performance of natural convection flat plate solar air collector with additional transparent insulation material parallel slats (TIM-PS), Solar Energy 231 (2022) 379–401.
[17] J. Alsarraf, et al., Turbulent forced convection and entropy production of a nanofluid in a solar collector considering various shapes for nanoparticles, Int. Commun. Heat Mass Transf. 117 (2020) 104804.
[18] K. Al-Farhany, et al., Magnetohydrodynamic double-diffusive mixed convection in a curvilinear cavity filled with nanofluid and containing conducting fins, Int. Commun. Heat Mass Transf. 144 (2023) 106802.
[19] K. Al-Farhany, et al., Numerical investigation of double-diffusive natural convection in a staggered cavity with two triangular obstacles, Eur. Phys. J. Plus 136 (8) (2021) 814.
[20] M.A. Alomari, et al., Numerical analysis of double-diffusive free convection in a curvilinear cavity filled with nanofluid and triple fins attached to the hot walls, Eur. Phys. J. Plus 139 (2) (2024) 149.
[21] N. Biswas, et al., Magneto-hydrothermal triple-convection in a W-shaped porous cavity containing oxytactic bacteria, Sci. Rep. 12 (1) (2022) 18053.
[22] D.K. Mandal, et al., Magneto-hydrothermal performance of hybrid nanofluid flow through a non-Darcian porous complex wavy enclosure, Eur. Phys. J. Spec. Top. 231 (13) (2022) 2695–2712.
[23] S.S. Shah, R.U. Haq, W. Al-Kouz, Mixed convection analysis in a split lid-driven trapezoidal cavity having elliptic shaped obstacle, Int. Commun. Heat Mass Transf. 126 (2021) 105448.
[24] T.H. Ruvo, et al., Mixed convection in an open T-shaped cavity utilizing the effect of different inflow conditions with Al2O3-water nanofluid flow, Results Eng. 17 (2023) 100862.
[25] T. Armaghani, et al., MHD mixed convection of localized heat source/sink in an Al2O3-Cu/water hybrid nanofluid in ʟ-shaped cavity, Alex. Eng. J. 60 (3) (2021) 2947–2962.
[26] P.-Y. Xiong, et al., Numerical simulation of mixed convection flow and heat transfer in the lid-driven triangular cavity with different obstacle configurations, Int. Commun. Heat Mass Transf. 123 (2021) 105202.
[27] E. Çolak, H.F. Öztop, Ö. Ekici, MHD mixed convection in a chamfered lid-driven cavity with partial heating, Int. J. Heat Mass Transf. 156 (2020) 119901.
[28] Q.R. Al-Amir, et al., Investigation of natural convection and entropy generation in a porous titled Z-staggered cavity saturated by TiO2-water nanofluid, Int. J. Thermofluids 19 (2023) 100395.
[29] Z. Al-Dulaimi, et al., Enhanced conjugate natural convection in a corrugated porous enclosure with Ag-MgO hybrid nanofluid, Int. J. Thermofluids 21 (2024) 100574.
[30] T. Armaghani, et al., MHD mixed convection flow and heat transfer in an open C-shaped enclosure using water-copper oxide nanofluid, Heat Mass Transf. 54 (6) (2018) 1791–1801.
[31] W. Zhou, et al., Lattice Boltzmann simulation of mixed convection of nanofluid with different heat sources in a double lid-driven cavity, Int. Commun. Heat Mass Transf. 97 (2018) 39–46.
[32] F. Selimefendigil, H.F. Öztop, Mixed convection in a two-sided elastic walled and SiO2 nanofluid filled cavity with internal heat generation: effects of inner rotating cylinder and nanoparticle's shape, J. Mol. Liq. 212 (2015) 509–516.
[33] R. Loni, et al., Thermal and exergy performance of a nanofluid-based solar dish collector with spiral cavity receiver, Appl. Therm. Eng. 135 (2018) 206–217.
[34] A.K. Kareem, et al., Numerical investigation of mixed convection heat transfer of nanofluids in a lid-driven trapezoidal cavity, Int. Commun. Heat Mass Transf. 77 (2016) 195–205.
[35] Z. Islam, et al., Unsteady periodic natural convection in a triangular enclosure heated sinusoidally from the bottom using CNT-water nanofluid, Results Eng. 14 (2022) 100376.
[36] A.A.A.A. Al-Rashed, et al., 3D magneto-convective heat transfer in CNT-nanofluid filled cavity under partially active magnetic field, Phys. E: Low-dimensional Syst. Nanostruct. 99 (2018) 294–303.
[37] R. Al-Sayegh, Influence of external magnetic field inclination on three-dimensional buoyancy-driven convection in an open trapezoidal cavity filled with CNT-Water nanofluid, Int. J. Mech. Sci. 148 (2018) 756–765.
[38] F.S. Oğlakkaya, C. Bozkaya, Unsteady MHD mixed convection flow in a lid-driven cavity with a heated wavy wall, Int. J. Mech. Sci. 148 (2018) 231–245.
[39] P. Barnoon, et al., MHD mixed convection and entropy generation in a lid-driven cavity with rotating cylinders filled by a nanofluid using two phase mixture model, J. Magn. Magn. Mater. 483 (2019) 224–248.
[40] S. Moolya, A. Satheesh, Role of magnetic field and cavity inclination on double diffusive mixed convection in rectangular enclosed domain, Int. Commun. Heat Mass Transf. 118 (2020).
[41] G.H.R. Kefayati, Double-diffusive natural convection and entropy generation of Bingham fluid in an inclined cavity, Int. J. Heat Mass Transf. 116 (2018) 762–812.
[42] Chamkha, A.J., F. Selimefendigil, and H.F. Oztop, MHD mixed convection and entropy generation in a lid-driven triangular cavity for various electrical conductivity models. 2018. 20(12): p. 903.
[43] Yuan, Z., Y. Dong, and Z. Jin, Numerical simulation of mhd natural convection and entropy generation in semicircular cavity based on LBM. 2023. 16(10): p. 4055.
[44] Sohut, F.H., et al., Mixed convection hybrid nanofluid flow induced by an inclined cylinder with lorentz forces. 2023. 14(5): p. 982.
[45] M. Hasan, et al., Influence of thermal conductivity on transient mixed convection in a vented cavity with a hollow cylinder and filled with CNT-water nanofluid, Heliyon 9 (3) (2023) e13850.
[46] S. Munawar, et al., Mixed convection of hybrid nanofluid in an inclined enclosure with a circular center heater under inclined magnetic field, Coatings 11 (5) (2021).
[47] P. Mondal, T.R. Mahapatra, MHD double-diffusive mixed convection and entropy generation of nanofluid in a trapezoidal cavity, Int. J. Mech. Sci. (2021) 208.
[48] P. Mondal, T.R. Mahapatra, R. Parveen, Entropy generation in nanofluid flow due to double diffusive MHD mixed convection, Heliyon, 7 (3) (2021) e06143.
[49] M. Siavashi, R. Yousofvand, S. Rezanejad, Nanofluid and porous fins effect on natural convection and entropy generation of flow inside a cavity, Adv. Powder Technol. 29 (1) (2018) 142–156.
[50] F.J. Gumir, et al., Natural convection in a porous cavity filled (35%MWCNT-65% Fe3O4)/water hybrid nanofluid with a solid wavy wall via Galerkin finite-element process, Sci. Rep. 12 (1) (2022) 17794.

[51] Bejan, A.J.J.o.A.P., Entropy generation minimization: the new thermodynamics of finite-size devices and finite-time processes. 1996. 79(3): p. 1191–1218.
[52] A. Bejan, A Study of Entropy Generation in Fundamental Convective Heat Transfer, J. Heat Transfer 101 (4) (1979) 718–725.
[53] R. Parveen, T.R. Mahapatra, Numerical simulation of MHD double diffusive natural convection and entropy generation in a wavy enclosure filled with nanofluid with discrete heating, Heliyon 5 (9) (2019) e02496.
[54] P. Mondal, T.R. Mahapatra, MHD double-diffusive mixed convection and entropy generation of nanofluid in a trapezoidal cavity, Int. J. Mech. Sci. 208 (2021) 106665.
[55] A. Abdulkadhim, et al., Effect of heat generation and heat absorption on natural convection of Cu-water nanofluid in a wavy enclosure under magnetic field, Int. Commun. Heat Mass Transf. 120 (2021) 105024.
[56] S.S. Shah, R.U. Haq, W. Al-Kouz, Mixed convection analysis in a split lid-driven trapezoidal cavity having elliptic shaped obstacle, Int. Commun. Heat Mass Transf. 126 (2021).
[57] B. Ghasemi, S.M. Aminossadati, A. Raisi, Magnetic field effect on natural convection in a nanofluid-filled square enclosure, Int. J. Therm. Sci. 50 (9) (2011) 1748–1756.